## Confinement Controls the Bend Instability of Three-Dimensional Active Liquid Crystals

Pooja Chandrakar<sup>®</sup>, <sup>1,2</sup> Minu Varghese, <sup>1</sup> S.Ali Aghvami<sup>®</sup>, <sup>1</sup> Aparna Baskaran<sup>®</sup>, <sup>1</sup> Zvonimir Dogic, <sup>2,1</sup> and Guillaume Duclos<sup>®</sup>, <sup>\*</sup> <sup>1</sup>Department of Physics, Brandeis University, Waltham, Massachusetts 02453, USA <sup>2</sup>Department of Physics, University of California at Santa Barbara, Santa Barbara, California 93106, USA



(Received 6 July 2020; revised 15 October 2020; accepted 11 November 2020; published 18 December 2020)

Spontaneous growth of long-wavelength deformations is a defining feature of active liquid crystals. We investigate the effect of confinement on the instability of 3D active liquid crystals in the isotropic phase composed of extensile microtubule bundles and kinesin molecular motors. When shear aligned, such fluids exhibit finite-wavelength self-amplifying bend deformations. By systematically changing the channel size we elucidate how the instability wavelength and its growth rate depend on the channel dimensions. Experimental findings are qualitatively consistent with a minimal hydrodynamic model, where the fastest growing deformation is set by a balance of active driving and elastic relaxation. Our results demonstrate that confinement determines the structure and dynamics of active fluids on all experimentally accessible length scales.

DOI: 10.1103/PhysRevLett.125.257801

Active fluids are internally driven nonequilibrium systems composed of motile constituents [1,2]. For active liquid crystals, energy-consuming rodlike units generate mesoscopic active stresses that are proportional to the local nematic order parameter. A dramatic consequence of extensile stresses is the intrinsic bend instability of aligned suspensions [3–7]. Orientational fluctuations generate self-amplifying deformations, which destroy long-range nematic order, leading to a dynamical steady state characterized by autonomous chaotic flows [8-13]. Boundaries and geometrical confinement can transform such inherently chaotic dynamics [14–23]. For example, three-dimensional annular channels convert chaotic flows into long-ranged coherent flows capable of transporting materials on meter scales, thus leading to potential long-term applications in microfluidics and soft robotics [23]. However, the exact mechanisms by which boundaries transform locally generated active stresses to power coherent flows remain under investigation. Two parallel planar walls are the simplest geometry to investigate boundary effects. Previous measurements of the characteristic length scale in 3D active fluids—including dense bacterial suspensions [8,24–26], living liquid crystals [10], and reconstituted cytoskeletal networks [9]—were performed in such geometries. However, rigorous testing of existing active hydrodynamic theories requires a quantitative relationship between confinement for a wide range of plate spacing and the resulting structure and dynamics of active fluids. Understanding active fluids in parallel plate geometry would provide a stepping stone for designing more complex boundaries that can control chaotic dynamics of active fluids. Hydrodynamic models predict that, in the absence of boundaries, uniformly aligned active nematics are unstable

at any nonzero activity, and that the fastest-growing deformation has an infinite wavelength [3,7]. Active stresses equally amplify orientational fluctuations at all length scales. Short-wavelength modes have higher elastic costs, hence the fastest growing mode has an infinite wavelength. Experimentally verifying this prediction remains a challenge. For example, previous studies examined this instability for microtubule-based 2D active nematics assembled on an oil-water-interface, but this leads to a fundamentally different wavelength selection mechanism as the viscous damping by the oil layer screens longrange hydrodynamic flows and prevents the growth of long-wavelength modes [27–31].

The unique properties of microtubule-based active matter allow for assembly of bulk 3D active liquid crystals in the absence of substrate friction. Using this feature, we investigate the instability of shear-aligned 3D active liquid crystals in the isotropic phase confined within microfluidic channels. Experiments demonstrate a boundary-dominated wavelength selection mechanism. We find that (i) the channel size determines the length scale of the growing deformations; (ii) boundaries set the dominant instability plane, and confinement in the direction normal to the instability plane controls the wavelength of the deformations; (iii) weakening confinement leads to larger wavelengths and faster dynamics; (iv) bulk dynamics cannot be reached as the active fluid structure is determined by the boundaries for all experimentally realizable geometries; and (v) the instability switches from an initially exponential to linear growth regime. The first four experimental findings are consistent with the linear stability analysis of a minimal hydrodynamic model. These results demonstrate the inherent challenge of using boundary-free

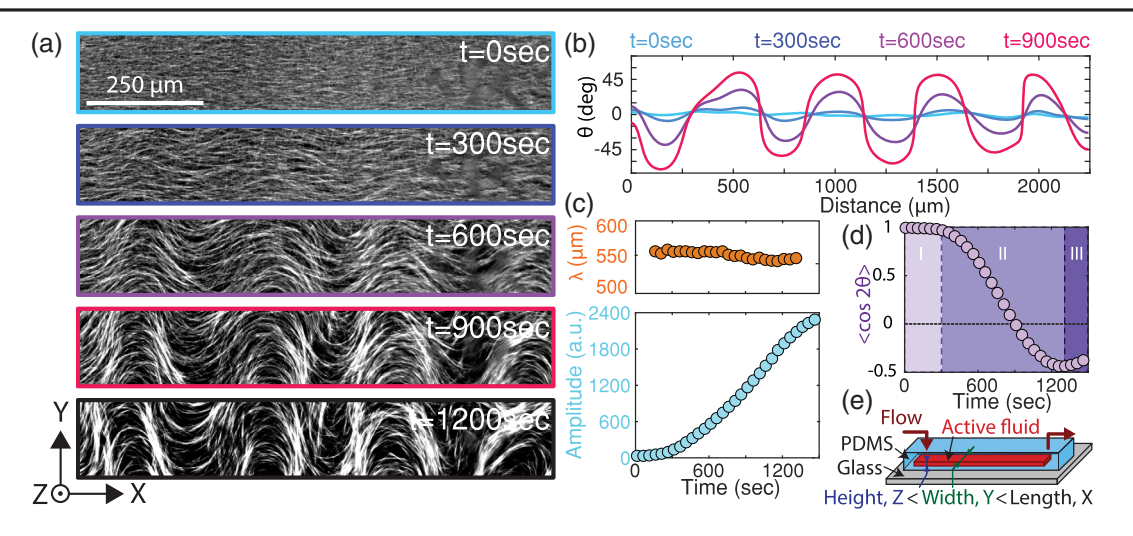


FIG. 1. Bend instability in confined microtubule-based active nematics. (a) Instability of the flow-aligned 3D microtubule-based active nematic in the isotropic phase (fluorescent microscopy). (b) Temporal evolution of the nematic director along the channel direction.  $\theta$  is the angle between the local nematic director and the channel's long axis (x axis). (c) Temporal evolution of the instability wavelength and amplitude. (d) Temporal evolution of the alignment parameter  $q = \langle \cos(2\theta) \rangle$ ; q quantifies the degree of ordering within a field of view. (e) Schematic of the microfluidic channels with rectangular cross-sections.  $H = 100 \ \mu m$ ,  $W = 3 \ mm$ , [KSA] = 10 nM.

calculations to explain experiments that, by necessity, have boundaries.

We study active fluids composed of rodlike microtubules (MT, ~0.1% volume fraction) bundled by a nonspecific depletant [9,32]. The MT bundle density is below the isotropic-nematic transition concentration; hence they form an active liquid crystal in the isotropic phase. The suspension is driven away from equilibrium by clusters of kinesin motors, which hydrolyze adenosine 5'-triphosphate (ATP) to step along and slide apart adjacent antiparallel microtubules. Such extensile units push fluid along both directions of their long axis while pulling fluid along their short axis. Hence, they exert dipolar extensile stresses [1]. The MT bundles form a continuously reconfiguring network that powers autonomous flows. Importantly, MT-based active fluids can be assembled in large quantities, allowing us to study the influence of boundaries on millimeter scales [33].

We confined the active fluid within microfabricated channels, whose heights (*H*, *z* axis) were either smaller or equal to their widths (*W*, *y* axis) [Fig. 1(e)]. We imposed a transient shear flow that uniformly aligns the active liquid crystal along the channel's length (*x* axis), similarly to passive rodlike colloids and shear-induced isotropic-nematic transition [34–37]. After the external flow ceased, such monodomains became unstable, exhibiting a robust growing pattern with spatially uniform wavelength [Figs. 1(a)–1(b), Supplemental Material [38], materials and methods, which includes Refs. [39–54], Movies S1, S2]. Since MT bundles are extensile, fluctuations about the aligned state generated unbalanced internal forces that acted on the surrounding fluid. The flows generated by the extensile activity self-amplified the initial bend

deformations, giving rise to a rapidly growing in-plane deformation pattern [4]. Instability required both ATP and a critical molecular motor concentration. In the highly confined regime (W = 2.5 mm,  $H = 100 \mu$ m), the instability was entirely suppressed for motor cluster concentrations less than 5 nM [Fig. S1, [38], Movie S3]. To quantify the instability, we measured both the temporal evolution of the in-plane velocity v and the nematic director  $\mathbf{n}[\cos(\theta), \sin(\theta)]$ , where  $\theta$  is the angle between the local bundle alignment and the channel's flow direction (x axis). Both the velocity and nematic director field exhibited periodic patterns from which we extracted the wavelength and the amplitude of the fastest growing mode (Fig. S2, [38]). The amplitude first grew exponentially, and then transitioned to a linear growth regime, which persisted until saturation [Fig. 1(c)]. The transition from exponential to linear growth was observed over a wide range of motor concentrations (Fig. S3, [38]).

The temporal evolution of the MT alignment was quantified by the alignment parameter  $q = \langle \cos(2\theta) \rangle$  [Fig. 1(d)]. During the exponential growth, MT-bundles were well aligned ( $q \sim 1$ ) along the channel's long axis. As the nematic director buckled, the bundles increasingly pointed along the y-axis, which led to a decreasing q. Eventually, the alignment parameter q became negative, reaching a minimum  $q \sim -0.5$ . At that point, growth slowed and the bundles were on average aligned along the y-axis. The resultant state, although not as ordered as the initial state, was itself unstable, leading to a second instability along the x-direction. Similar to 2D nematics [55], a cascade of instabilities orthogonal to each other ensued (Fig. S4 [38]). This cascade of instabilities melted the initially shear aligned nematic phase into the previously

studied active isotropic liquid crystal [9]. The wavelength of the successive instabilities increased over time until the fluid reached its chaotic steady-state. The wavelength increase could be due to an increase of the elastic constant from the coarsening of the MT-bundles, and/or a decrease of the degree of ordering of the successive aligned states prior to each instability cycle (Fig. S4E [38]).

The instability can be modeled by the linearized equations of 3D active nemato-hydrodynamics for an extensile nematic liquid crystal (Supplemental Material [38]) [3]. In the absence of boundaries, the fastest growing mode at any nonzero activity corresponds to pure-bend deformations and the instability wavelength is infinite. Introducing no-slip hydrodynamic boundaries without assuming any specific anchoring of the nematic director changes several features of the instability. First, the active nematic is unstable only if the activity is above a critical value, similar to confined 2D active nematics (Fig. S1 [38]) [4,6,19,56]. Second, above that threshold, there is a finite range of unstable wavelengths. These predictions are in agreement with the experimental findings. Furthermore, theory predicts that for confined 3D active nematics both twist-bend and splay-bend modes are unstable, with the former having faster growth (Supplemental Material [38]). To verify the last prediction, we imaged the MT-bundles with confocal microscopy. These experiments confirmed that the 3D instability was not pure-bend, as the in-plane director was not uniform at different z-planes (Fig. S5 [38]). Moreover, the in-plane bend deformations of the MT-bundles grew faster than the in-plane splay deformations (Fig. S6 [38]).

Further, the model also makes a prediction about the instability direction. In bulk active fluids, orientation fluctuations are isotropic. When confined, the linear stability analysis revealed that the unstable twist-bend modes are given by  $\mathbf{x}.(\mathbf{k} \times \delta \mathbf{n}_{\perp}) \propto \delta n_z / W - \delta n_v / H$ , where k is the wave vector of the unstable mode, and  $\delta n_{\perp} = (\delta n_y, \delta n_z)$  is a sinusoidal perturbation perpendicular to the channel's direction (Supplemental Material [38]). If  $H \ll W$ , the unstable mode consists predominantly of  $\delta n_{\rm v}$ . This is consistent with experiments: spontaneous growth of deformations was most conspicuous in the image (x-y) plane, which is orthogonal to the strongest confinement direction (z axis) [Fig. 1(a)]. For channels with a square cross-section, the linear stability analysis predicts that the deformations will grow equally fast in both confinement directions (y and z axis).

So far, we described the instability of initially shearaligned active liquid crystals in the highly confined regime (H = 0.1 mm, W = 3 mm). Next, we systematically changed the channel's width and height to determine how the confinement size controls the wavelength selection mechanism. We started by increasing the channel height (H, z direction) from 0.1 to 3 mm while keeping its width (W, y direction) fixed at 3 mm (Movie S6, [38]). Confocal

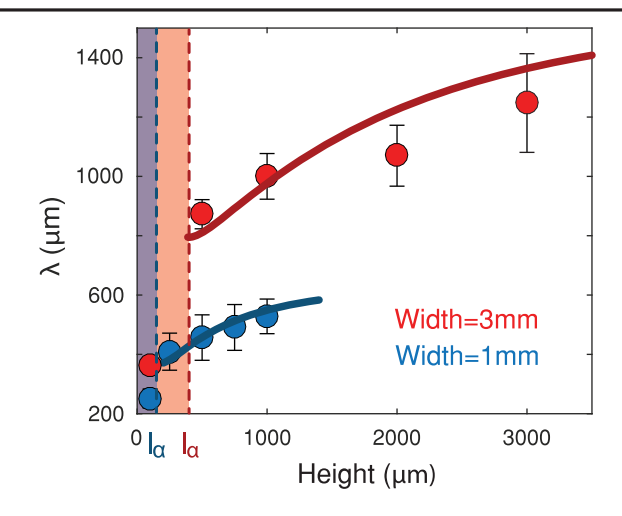


FIG. 2. Channel's dimensions set the instability wavelength: evolution of the wavelength instability as a function of channel height. Symbols correspond to experimental data points and solid lines to theoretical fits for  $\ell_{\alpha}(3 \text{ mm}) = 400 \ \mu\text{m}$  and  $\ell_{\alpha}(1 \text{ mm}) = 150 \ \mu\text{m}$ . The active length is different for each data set because the experiments were realized with different batch of microtubules that have different activity level. Shaded areas show where the theory predicts no instability. Error bars show standard deviation. ([KSA] = 120 nM).

images of labeled MTs confirmed that the bundles were uniformly aligned for all confinements (Movie S5, [38]). The instability wavelength and the associated growth rate strongly depended on the channel height, increasing rapidly for small channels (H < 1 mm) before plateauing for the larger channels [Fig. 2, Fig. S7A [38]]. Repeating these experiments for smaller widths showed that a combination of both the width and height sets the fastest growing mode [W = 1 mm, Fig. 2].

We next compare the confinement-dependent instability wavelength to the predictions of the linear stability analysis of our minimal hydrodynamic model with no-slip boundary and no specific anchoring of the nematic director at the walls. The model predicts that uniform nematic alignment is unstable when the confinement length scale  $L = (1/W^2 + 1/H^2)^{\frac{-1}{2}}$  is larger than the active lengthscale  $\ell_{\alpha} = 2\pi \sqrt{2\eta D_R \kappa / \alpha (S_0 + \xi)}$ , Supplemental Material [38]. Here,  $\alpha$  is the magnitude of the extensile force dipole generated by the MT-bundles,  $S_0$  is the magnitude of initial order,  $\xi$  is the flow alignment parameter,  $\eta$  is the viscosity,  $D_R$  is the rotational diffusion constant, and  $\kappa$  is the nematic elasticity. The wavelength of the fastest growing mode,  $\lambda$ , depends on the channel dimensions as:  $\lambda = 2[2/l_{\alpha}L - 1/L^2]^{\frac{-1}{2}}$ , Supplemental Material [38]. As the channel goes from a rectangular to a square cross-section, the theoretical scaling of the instability wavelength with the channel size agrees quantitatively with the experimental observations for L = 0.5-3 mm (Fig. 2). Furthermore, both experiments and theory demonstrate that the wavelength and the growth rate were mainly determined by the smaller channel dimensions and did not significantly change with increasing the larger channel dimension (Fig. S8, Fig. S7B, Movie S7 [38]). Finally, for channels where  $H, W \gg \ell_{\alpha}$ , the linear stability analysis predicts that  $\lambda \propto \sqrt{h/\sqrt{1+h^2}}.\sqrt{W}$ , where h=H/W is the aspect ratio of the channel's cross-section.

Theory and experiments quantitatively agree for the large channels' cross-sections, illustrating that the growing deformations in shear-aligned suspension of extensile MT-bundles is the long-wavelength hydrodynamic instability [3]. However, it is important to note some inconsistencies between the theory and the experiments. First, in the highly confined regime (L < 0.4 mm, W = 3 mm) the MT suspension was always unstable even, for L = 0.04 mm (Fig. 2). Fitting the hydrodynamic theory to the experimental data for L > 0.5 mm predicts no instability for channel sizes smaller than  $\ell_{\alpha} \sim 0.4$  mm. Highly confined suspensions of active MT might display shorter wavelength than allowed theoretically because the shear-aligned liquid crystal is below the Isotropic/Nematic transition, while the model assumes local nematic interactions at all time. Alternativity, the hydrodynamic model might require additional terms to describe the instability in the strong confinement regime (H, W < 0.4 mm). Second, the active length  $\ell_{\alpha}$  is a material constant that should not depend on confinement, unlike what we observe when fitting the model to the two data sets. We suspect that the difference  $\ell_{\alpha}$  obtained two different channel widths [blue and red dotted line in Fig. 2] is due to variability in the sample preparation protocols, which often result in samples a different activity.

Many existing experimental realizations of active matter—from shaken granular rods to multicellular tissues—are two dimensional. Motility in 2D often requires contact with a fluid or a solid substrate, which screens long-range hydrodynamic flows. Such screening can also result in instabilities with a finite wavelength [28,55]. The agreement between theory and experiments confirms that this instability is scale-free in bulk 3D active nematics and that the finite wavelength selection mechanism under confinement is fundamentally different from the overdamped instability reported in MT-based 2D active nematics moving on an oil-water interface [55]. The finite wavelength studied here is solely due to the presence of boundaries that impose constraints on the activity-driven flows. In the absence of boundaries, the most unstable mode is pure-bend with an infinite wavelength. Confinement in the direction of initial order (x-axis) restricts the maximum allowed wavelength so that the most unstable mode is a pure-bend mode with a wavelength equal to the system size. For confinements perpendicular to the direction of initial order (y and z axis), such as those studied here, the presence of no-slip boundaries constraints the velocity and director fields such that deformations are no longer pure-bend but

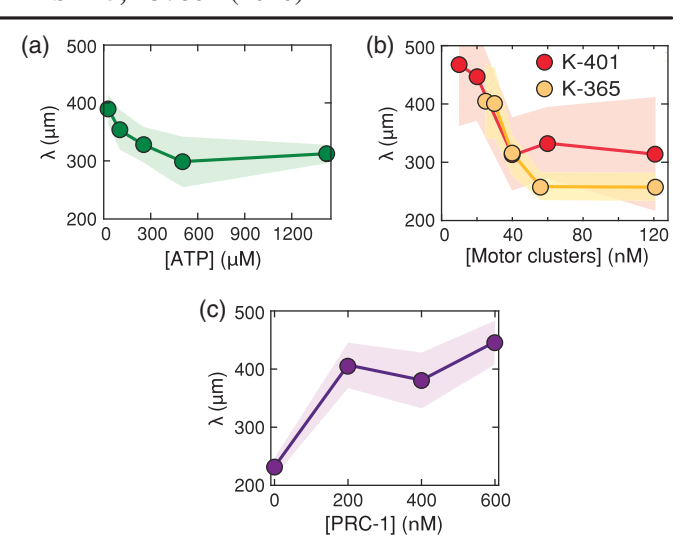


FIG. 3. Molecular control of the instability wavelength in the highly confined regime. Dependence of the instability wavelength for varying concentrations of (a) adenosine-5'-triphosphate (ATP), (b) molecular motor clusters (processive K-401 and nonprocessive K-365) and (c) MT-crosslinkers PRC-1. Shaded areas show standard deviation. W=3 mm,  $H=100~\mu m$ .

contain splay and twist. Long-wavelength bend deformations are suppressed because the active driving cannot overcome the viscous and elastic costs that come with the associated but energetically costly splay and twist deformations. Short-wavelength modes have a larger fraction of pure bend; hence activity destabilizes these modes more than the longer-wavelength modes. Shortest wavelength modes are again stabilized by elasticity and viscous dissipation. Consequently, this competition between active and dissipative processes implies that the fastest growing mode has a non-trivial finite wavelength.

So far, we demonstrated that the channel size controls both the growth rate and the wavelength of the instability. Next, we control the instability wavelength by tuning the intrinsic material properties of an active fluid, such as the activity or the network elasticity. Linear stability analysis predicts that the fluid becomes unstable at length scales larger than  $l_{\alpha} \propto \sqrt{\kappa/\alpha}$ , where  $\kappa$  is the sample elasticity, and  $\alpha$  is the activity coefficient (Supplemental Material [38]) [12,57]. For strong confinements (W=3mm,  $H = 100 \mu \text{m}$ ), the wavelength slightly decreases with increasing ATP concentration [Fig. 3(a)]. It is often assumed that ATP controls the magnitude of the active stress. However, this dependency does not necessarily account for the biochemistry behind kinesin stepping: processive motors take multiple steps on a microtubule before unbinding. After most steps, the motor waits for the ATP molecule to bind before taking the next step [58]. Clusters of processive motors can bind to multiple microtubules and therefore have a dual role, acting both as passive cross-linkers and generators of active stresses [59]. With decreasing ATP, kinesin dwell time increases, and motor clusters spend an increasing amount of time passively cross-linking the MT-bundles while waiting for ATP binding [58]. In the limit of zero ATP, kinesin clusters passively crosslink the filaments, yielding a solid-like material [60]. These considerations hinder the simple interpretation of how the instability wavelength depends on the activity because tuning ATP concentration changes both the activity and elasticity.

To overcome the above-mentioned complexities, we titrated the concentrations of motor clusters at saturating ATP concentrations. The instability wavelength decreased sharply with increasing motor concentration [Fig. 3(b)]. Second, we repeated the same experiment with clusters of non-processive K365 motors that detach from the MT after each step. We again observed decreasing wavelength with increasing motor concentration [Fig. 3(b)]. This is consistent with an increase of the activity  $\alpha$ . To explore the influence of elasticity, we kept the kinesin concentration constant while adding a varying amount of PRC-1, a specific crosslinker that bundles antiparallel microtubules while still allowing for their relative sliding [33,44]. Generally, increasing the number of crosslinkers should lead to stiffer bundles [61]. In agreement with this expectation, we find that increasing PRC-1 concentration increased the instability wavelength [Fig. 3(c)]. As we did not change the number of stress-generating motors, this is consistent with an increase of the sample elasticity  $\kappa$ . Taken together, these experiments confirm that in the highly confined regime, the instability wavelength is determined by the balance of active and elastic stresses, which are respectively controlled by the concentration of stress generating motors and non-motor crosslinkers.

To summarize, above a critical concentration of molecular motors, shear-aligned 3D active liquid crystals in the isotropic phase composed of extensile MT bundles exhibit an activity driven hydrodynamic instability. The fastest-growing mode has a finite wavelength that is determined by confinement geometry and material properties. The observed scaling with the confinement size is consistent with a minimal hydrodynamic model, which predicts that the instability wavelength will be infinite in the bulk limit. However, reaching this limit is an experimental challenge. For square channels that are much larger than the critical length, the instability wavelength grows slower than the system size:  $\lambda \propto \sqrt{W}$ . Such weak scaling indicates that the active fluid structure is determined by the presence of boundaries, no matter how far they are from each other. We demonstrated that the instability wavelength is set by the balance of active and elastic stresses, which are independently controlled by the concentration of motors and non-motile crosslinkers. Changing ATP concentration is not a good control over the activity parameter often found in theoretical models because it affects both the magnitude of the active stress and the dwelling time of motors that crosslinking MT bundles. We consider these findings in the context of the previously published results. First, a similar instability was observed in kinesin-free MT suspension, where the extensile stress was generated by the filament growth [62]. Intriguingly, out-of-plane motor-driven buckling was reported for suspensions of longer MTs and lower motor concentrations [63,64], which suggests a more solid-like character of the MT network in this regime, a hypothesis also investigated by rheology [60]. Second, for MT active isotropic fluids, velocity-velocity correlation length in the chaotic state were performed in wide but thin microscopy chambers ( $H \sim 100 \ \mu \text{m}$ ) [9,32]. Results shown here indicate that such measurements were influenced by the boundaries and are not representative of bulk dynamics. Third, the ability of 3D active fluids to adjust their internal structure in response to changing boundaries provides new insights required for understanding the scale-invariant criterion that determines the onset of long-range transport flows in confined active fluids [23,65,66]. Taken together, our combined experimental and theoretical findings advance understanding of both the pathways to low Reynold number 3D active turbulence and how such pathways are affected by boundaries [13].

We thank Bezia Lemma, Radhika Subramanian, and Marc Ridilla for their help in protein purification. P. C. and Z. D. acknowledge support of Department of Energy, Office of Basic Energy Sciences under Award No. DE-SC0019733. We also acknowledge the use of the optical, microfluidics, and biomaterial facilities supported by NSF MRSEC DMR-2011846. G. D., M. V., S. A. A., and A. B. acknowledge support of NSF MRSEC DMR-2011846. G. D acknowledges support from Brandeis University. A. B acknowledges funding from US-Israel Binational Science Foundation through BSF-2014279.

<sup>\*</sup>Corresponding author. gduclos@brandeis.edu

M. C. Marchetti, J.-F. Joanny, S. Ramaswamy, T. B. Liverpool, J. Prost, M. Rao, and R. A. Simha, Hydrodynamics of soft active matter, Rev. Mod. Phys. 85, 1143 (2013).

<sup>[2]</sup> S. Ramaswamy, Active fluids, Nat. Rev. Phys. **1**, 640 (2019).

<sup>[3]</sup> R. A. Simha and S. Ramaswamy, Hydrodynamic fluctuations and instabilities in ordered suspensions of self-propelled particles, Phys. Rev. Lett. **89**, 058101 (2002).

<sup>[4]</sup> S. Ramaswamy and M. Rao, Active-filament hydrodynamics: instabilities, boundary conditions and rheology, New J. Phys. **9**, 423 (2007).

<sup>[5]</sup> T. B. Liverpool and M. C. Marchetti, Instabilities of Isotropic Solutions of Active Polar Filaments, Phys. Rev. Lett. 90, 138102 (2003).

<sup>[6]</sup> D. Marenduzzo, E. Orlandini, and J. M. Yeomans, Hydrodynamics and Rheology of Active Liquid Crystals:

- A Numerical Investigation, Phys. Rev. Lett. **98**, 118102 (2007).
- [7] D. Saintillan and M. J. Shelley, Instabilities and Pattern Formation in Active Particle Suspensions: Kinetic Theory and Continuum Simulations, Phys. Rev. Lett. 100, 178103 (2008).
- [8] J. Dunkel, S. Heidenreich, K. Drescher, H. H. Wensink, M. Bar, and R. E. Goldstein, Fluid Dynamics of Bacterial Turbulence, Phys. Rev. Lett. 110, 228102 (2013).
- [9] T. Sanchez, D. T. Chen, S. J. DeCamp, M. Heymann, and Z. Dogic, Spontaneous motion in hierarchically assembled active matter, Nature (London) 491, 431 (2012).
- [10] S. Zhou, A. Sokolov, O. D. Lavrentovich, and I. S. Aranson, Living liquid crystals, Proc. Natl. Acad. Sci. U.S.A. 111, 1265 (2014).
- [11] C. Blanch-Mercader, V. Yashunsky, S. Garcia, G. Duclos, L. Giomi, and P. Silberzan, Turbulent Dynamics of Epithelial Cell Cultures, Phys. Rev. Lett. 120, 208101 (2018).
- [12] L. Giomi, Geometry and Topology of Turbulence in Active Nematics, Phys. Rev. X 5, 031003 (2015).
- [13] R. Alert, J.-F. Joanny, and J. Casademunt, Universal scaling of active nematic turbulence, Nat. Phys. 16, 682 (2020).
- [14] A. Bricard, J.-B. Caussin, N. Desreumaux, O. Dauchot, and D. Bartolo, Emergence of macroscopic directed motion in populations of motile colloids, Nature (London) 503, 95 (2013).
- [15] H. Wioland, F. G. Woodhouse, J. Dunkel, J. O. Kessler, and R. E. Goldstein, Confinement stabilizes a bacterial suspension into a spiral vortex, Phys. Rev. Lett. 110, 268102 (2013).
- [16] D. Nishiguchi, I. S. Aranson, A. Snezhko, and A. Sokolov, Engineering bacterial vortex lattice via direct laser lithography, Nat. Commun. 9, 1 (2018).
- [17] A. Opathalage, M. M. Norton, M. P. Juniper, B. Langeslay, S. A. Aghvami, S. Fraden, and Z. Dogic, Self-organized dynamics and the transition to turbulence of confined active nematics, Proc. Natl. Acad. Sci. U.S.A. 116, 4788 (2019).
- [18] M. Theillard, R. Alonso-Matilla, and D. Saintillan, Geometric control of active collective motion, Soft Matter 13, 363 (2017).
- [19] R. Voituriez, J.-F. Joanny, and J. Prost, Spontaneous flow transition in active polar gels, Europhys. Lett. **70**, 404 (2005).
- [20] A. P. Berke, L. Turner, H. C. Berg, and E. Lauga, Hydrodynamic Attraction of Swimming Microorganisms By Surfaces, Phys. Rev. Lett. 101, 038102 (2008).
- [21] A. Doostmohammadi, T. N. Shendruk, K. Thijssen, and J. M. Yeomans, Onset of meso-scale turbulence in active nematics, Nat. Commun. 8, 15326 (2017).
- [22] T. N. Shendruk, A. Doostmohammadi, K. Thijssen, and J. M. Yeomans, Dancing disclinations in confined active nematics, Soft Matter 13, 3853 (2017).
- [23] K.-T. Wu, J. B. Hishamunda, D. T. Chen, S. J. DeCamp, Y.-W. Chang, A. Fernández-Nieves, S. Fraden, and Z. Dogic, Transition from turbulent to coherent flows in confined three-dimensional active fluids, Science 355, eaal1979 (2017).
- [24] A. Sokolov, R. E. Goldstein, F. I. Feldchtein, and I. S. Aranson, Enhanced mixing and spatial instability in

- concentrated bacterial suspensions, Phys. Rev. E **80**, 031903 (2009).
- [25] V. A. Martinez *et al.*, A combined rheometry and imaging study of viscosity reduction in bacterial suspensions, Proc. Natl. Acad. Sci. U.S.A. **117**, 2326 (2020).
- [26] S. Guo, D. Samanta, Y. Peng, X. Xu, and X. Cheng, Symmetric shear banding and swarming vortices in bacterial superfluids, Proc. Natl. Acad. Sci. U.S.A. 115, 7212 (2018).
- [27] M. Leoni and T. B. Liverpool, Swimmers in Thin Films: From Swarming to Hydrodynamic Instabilities, Phys. Rev. Lett. **105**, 238102 (2010).
- [28] S. P. Thampi, R. Golestanian, and J. M. Yeomans, Active nematic materials with substrate friction, Phys. Rev. E **90**, 062307 (2014).
- [29] T. Gao, R. Blackwell, M. A. Glaser, M. D. Betterton, and M. J. Shelley, Multiscale Polar Theory of Microtubule and Motor-Protein Assemblies, Phys. Rev. Lett. 114, 048101 (2015).
- [30] E. Putzig, G. S. Redner, A. Baskaran, and A. Baskaran, Instabilities, defects, and defects ordering in an overdamped active nematic, Soft Matter 12, 3854 (2016).
- [31] T. Gao, M. D. Betterton, A.-S. Jhang, and M. J. Shelley, Analytical structure, dynamics, and coarse graining of a kinetic model of an active fluid, Phys. Rev. Fluids 2, 093302 (2017).
- [32] G. Henkin, S. J. DeCamp, D. T. Chen, T. Sanchez, and Z. Dogic, Tunable dynamics of microtubulebased active isotropic gels, Phil. Trans. R. Soc. A **372**, 20140142 (2014).
- [33] P. Chandrakar *et al.*, Microtubule-based active fluids with improved lifetime, temporal stability and miscibility with passive soft materials, arXiv:1811.05026.
- [34] S. Hess, Pre-and post-transitional behavior of the flow alignment and flow-induced phase transition in liquid crystals, Z. Naturforsch. A **31a**, 1507 (1976).
- [35] P. D. Olmsted and P. M. Goldbart, Isotropic-nematic transition in shear flow: State selection, coexistence, phase transitions, and critical behavior, Phys. Rev. A **46**, 4966 (1992).
- [36] C. Lang, J. Kohlbrecher, L. Porcar, A. Radulescu, K. Sellinghoff, J. K. G. Dhont, and M. P. Lettinga, Microstructural understanding of the length-and stiffness-dependent shear thinning in semidilute colloidal rods, Macromolecules 52, 9604 (2019).
- [37] T. A. J. Lenstra, Z. Dogic, and J. K. G. Dhont, Shear-induced displacement of isotropic-nematic spinodals, J. Chem. Phys. **114**, 10151 (2001).
- [38] See Supplemental Material at http://link.aps.org/supplemental/10.1103/PhysRevLett.125.257801 for by Materials and methods, theoretical models, supplementary figures and description of the supplementary movies.
- [39] M. Castoldi and A. V. Popov, Purification of brain tubulin through two cycles of polymerization—depolymerization in a high-molarity buffer, Protein Expression Purif. **32**, 83 (2003).
- [40] A. Hyman, D. Drechsel, D. Kellogg, S. Salser, K. Sawin, P. Steffen, L. Wordeman, and T. Mitchison, in, *Methods in Enzymology* (Academic Press, New York, 1991), p. 478.
- [41] S. J. DeCamp, G. S. Redner, A. Baskaran, M. F. Hagan, and Z. Dogic, Orientational order of motile defects in active nematic, Nat. Mater. **14**, 1110 (2015).
- [42] D. S. Martin, R. Fathi, T. J. Mitchison, and J. Gelles, FRET measurements of kinesin neck orientation reveal a structural

- basis for processivity and asymmetry, Proc. Natl. Acad. Sci. U.S.A. **107**, 5453 (2010).
- [43] E. C. Young, H. K. Mahtani, and J. Gelles, One-headed kinesin derivatives move by a nonprocessive, low-duty ratio mechanism unlike that of two-headed kinesin, Biochemistry 37, 3467 (1998).
- [44] R. Subramanian, E. M. Wilson-Kubalek, C. P. Arthur, M. J. Bick, E. A. Campbell, S. A. Darst, R. A. Milligan, and T. M. Kapoor, Insights into antiparallel microtubule crosslinking by PRC1, a conserved nonmotor microtubule binding protein, Cell 142, 433 (2010).
- [45] S. A. Aghvami, A. Opathalage, Z. K. Zhang, M. Ludwig, M. Heymann, M. Norton, N. Wilkins, and S. Fraden, Rapid prototyping of cyclic olefin copolymer (COC) microfluidic devices, Sens. Actuators B 247, 940 (2017).
- [46] M. A. Unger, H.-P. Chou, T. Thorsen, A. Scherer, and S. R. Quake, Monolithic microfabricated valves and pumps by multilayer soft lithography, Science 288, 113 (2000).
- [47] A. D. Edelstein, M. A. Tsuchida, N. Amodaj, H. Pinkard, R. D. Vale, and N. Stuurman, Advanced methods of microscope control using muManager software, J. Biol. Methods 1 (2014).
- [48] C. A. Schneider W. S. Rasband, and K. W. Eliceiri, NIH Image to ImageJ: 25 years of image analysis, Nat Methods 9, 671 (2012).
- [49] MATLAB, version 7.10.0 (R2010a) (The MathWorks Inc., Natick, Massachusetts, 2010).
- [50] R. Rezakhaniha, A. Agianniotis, J. T. Schrauwen, A. Griffa, D. Sage, C. V. Bouten, F. N. van de Vosse, M. Unser, and N. Stergiopulos, Experimental investigation of collagen waviness and orientation in the arterial adventitia using confocal laser scanning microscopy, Biomech. Model. Mechanobiol. 11, 461 (2012).
- [51] L. Petitjean, M. Reffay, E. Grasland-Mongrain, M. Poujade, B. Ladoux, A. Buguin, and P. Silberzan, Velocity fields in a collectively migrating epithelium, Biophys. J. 98, 1790 (2010).
- [52] P.-G. de Gennes and J. Prost, *The Physics of Liquid Crystals*, 2nd ed., International Series of Monographs on Physics (Oxford University Press, Clarendon Press, Oxford, New York, (1998).
- [53] A. Beris and B. Edwards, *Thermodynamics of Flowing Systems: With Internal Microstructure*(Oxford University Press, New York, 1994).

- [54] G. I. Taylor, The motion of ellipsoidal particles in a viscous fluid, Proc. R. Soc. A 103, 58 (1923), http://www.jstor.org/ stable/94096.
- [55] B. Martínez-Prat, J. Ignés-Mullol, J. Casademunt, and F. Sagués, Selection mechanism at the onset of active turbulence, Nat. Phys. **15**, 362 (2019).
- [56] G. Duclos, C. Blanch-Mercader, V. Yashunsky, G. Salbreux, J. F. Joanny, J. Prost, and P. Silberzan, Spontaneous shear flow in confined cellular nematics, Nat. Phys. 14, 728 (2018).
- [57] S. P. Thampi, R. Golestanian, and J. M. Yeomans, Vorticity, defects and correlations in active turbulence, Phil. Trans. R. Soc. A 372, 20130366 (2014).
- [58] M. J. Schnitzer and S. M. Block, Kinesin hydrolyses one ATP per 8-nm step, Nature (London) 388, 386(1997).
- [59] L. M. Lemma, S. J. DeCamp, Z. You, L. Giomi, and Z. Dogic, Statistical properties of autonomous flows in 2D active nematics, Soft Matter 15, 3264 (2019).
- [60] D. A. Gagnon, C. Dessi, J. P. Berezney, R. Boros, D. T. N. Chen, Z. Dogic, and D. L. Blair, Induced Gelation of Self-Yielding Active Networks, Phys. Rev. Lett. 125, 178003 (2020).
- [61] C. Heussinger, M. Bathe, and E. Frey, Statistical Mechanics of Semiflexible Bundles of Wormlike Polymer Chains, Phys. Rev. Lett. 99, 048101 (2007).
- [62] Y. Liu, Y. Guo, J. M. Valles, Jr., and J. X. Tang, Microtubule bundling and nested buckling drive stripe formation in polymerizing tubulin solutions, Proc. Natl. Acad. Sci. U.S.A. 103, 10654 (2006).
- [63] A. Senoussi, S. Kashida, R. Voituriez, J. C. Galas, A. Maitra, and A. Estevez-Torres, Tunable corrugated patterns in an active nematic sheet, Proc. Natl. Acad. Sci. U.S.A. 116, 22464 (2019).
- [64] T. Strubing, A. Khosravanizadeh, A. Vilfan, E. Bodenschatz, R. Golestanian, and I. Guido, Ramin Golestanian, I. Guido, Wrinkling instability in 3D active nematics, Nano Lett. 20, 6281 (2020).
- [65] S. Chandragiri, A. Doostmohammadi, J. M. Yeomans, and S. P. Thampi, Flow States and Transitions of an Active Nematic in a Three-Dimensional Channe, Phys. Rev. Lett. 125, 148002 (2020).
- [66] M. Varghese, A. Baskaran, M. F. Hagan, and A. Baskaran, Confinement-Induced Self-Pumping in 3D Active Fluids, Phys. Rev. Lett. (2020).